EFFECTS OF HIGH SALINITY WASTEWATER ON THE PROPERTIES OF COAL GASIFICATION RESIDUE-BASED CEMENTITIOUS MATERIAL

by

Feng WU and Hui LI [*]

School of Materials Science and Engineering, Xi'an University of Architecture and Technology,
Xi'an, China

Original scientific paper
https://doi.org/10.2298/TSCI2106161W

High salinity wastewater and coal gasification residue are the by-products which need to be utilized as resources for the sustainable development of coal-to-chemicals technology. Using coal gasification residue as the main raw material, supplemented with 10% Portland cement, and high salinity wastewater as the mixing water instead of tap water to prepare cementitious materials. The XRD, TG-DTG, FTIR, SEM, and MIP were used to analyze the influence mechanism of high salinity wastewater on the properties of cementitious materials. The results show that high salinity wastewater was beneficial to the strength development of the cementitious material. When 25% high salinity mastewater was used instead of tap water, the enhancing rates of compressive strength was 294%, 177%, and 186% curing at 3, 7, and 28 days. This is main due to the sulfate and chloride in the high salinity wastewater can promote the formation of C-S-H gels, Friedel's, salts and C-A-S-H gels in the hydration process of pastes, which can promote the densification of structure. The pores distribution and structure were optimized, increasing the proportion of capillary pores and decreasing macropore to promote the micro-structure more dense. This study can provide a new idea for the comprehensive utilization of industrial waste and achieve the purpose of "waste control by waste".

Key words*: coal-to-chemicals technology, high salinity wastewater, coal gasification residue, mixing water, compressive strength*

Instructions

The amount of coal gasification residue (CGR) and high salinity wastewater (HSW) is huge, which has become an important factor restricting the sustainable development of coal gasification industry [1]. Pomykala [2] has replaced all or part of the aggregate used for concrete with CGR. Acosta *et al*. [3] at the University of Castilla La Mancha in Spain studied the basic characteristics of CGR and its application in the preparation of lightweight porous aggregate and building bricks. American Praxis Engineers Co., Ltd. used the specific thermal expansion characteristics of CGR to prepare lightweight aggregate. The main components of

---

[*] Corresponding author, e-mail: sunshine_lihui@126.com

CGR are oxides such as SiO_2, Al_2O_3, Fe_2O_3, CaO, *etc*., [4]. Thus the slag has potential chemical activity [5]. So the slag components can be used to prepare ecological cementitious materials.

The HSW contains mainly sulfates and chlorides so that it can be used as mixing water for cementitious materials. At present, HSW is mainly used for the preparation of chemical by-products using evaporation and crystallization processes [6], Mei *et al*. [7] shows that Na_2SO_4 can improve the pore structure of fly ash better than can nano-SiO_2, and it promotes the hydration of cement. Shi and Day [8] reports that adding a small amount of Na_2SO_4 and $CaCl_2$ can increase the pozzolanic effect of fly ash. In addition, the pH of HSW is 9.6 and alkalinity is beneficial to the depolymerization of CGR, and then improving dissolution of active Si and Al to participate in the hydration reaction.

Using CGR as the main raw material, supplemented with 10% Portland cement, and HSW as the mixing water instead of tap water to prepare cementitious materials, the corresponding mechanism for the formation of hydration products and micro-structures was identified. The results provide guiding principle for the application of cementitious materials made from HSW instead of tap water.

Materials and methods

Raw materials

The raw materials used in this experiment include CGR, Portland 42.5 cement, HSW, and tap water. CGR and HSW were provided by Shenhua Ningxia Coal Industry Group Co., Ltd. The surface area of CGR was 380 m^2/kg, and its chemical and mineral composition are shown in tab. 1 and fig. 1. The chemical composition and mineral phase analysis of HSW were shown in tab. 2 and fig. 2.

Table 1. Chemical composition of CGR and Portland cement (wt.%)

Materials	SiO_2	Al_2O_3	CaO	Fe_2O_3	MgO	Na_2O	K_2O	TiO_2	SO_3	LOI
CGR	48.75	20.05	10.69	9.67	2.84	1.65	2.11	1.01	0.56	1.52
Portland cement	21.78	4.21	60.88	2.77	2.51	0.80	0.91	0.80	2.87	2.05

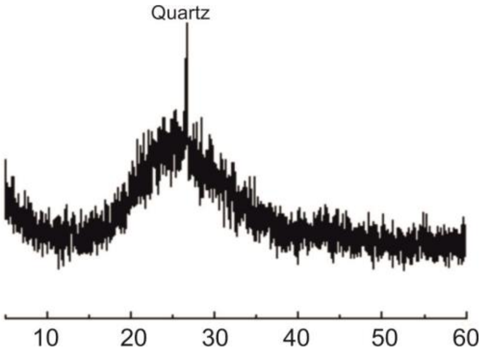

Figure 1. The XRD pattern of CGR

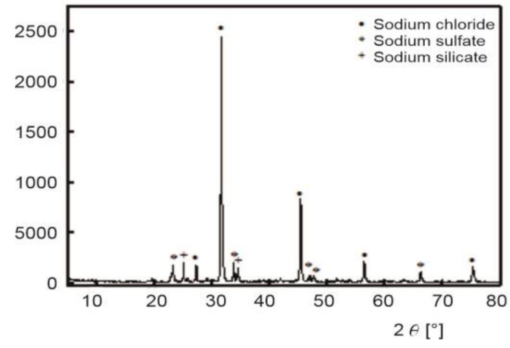

Figure 2. The XRD pattern of HSW

Table 2. The composition of HSW [molL^{-1}]

Salty species	Sulfate	Chloride	Phosphate	Nitrate	Nitrite	Ammonia salt	PH
Content	61.44	84.7	21.1	1145	92.34	25.58	9.6

The chemical components of CGR are mainly SiO_2, Al_2O_3, CaO, Fe_2O_3, and MgO, the phase of the CGR is mainly amorphous glass as indicated by the hump between 15°-35°, and it contains a small amount of the quartz phase (SiO_2) (2θ). As shown in tab. 2 and fig. 2, the solid content of HSW is about 21.78%, and it is mainly composed of sodium chloride, sulphate, and silicate with a pH value of 9.6.

Test method for paste

Cement, 10% by weight, was added to the CGR and mixed evenly. Sufficient water was weighed out to establish a 0.42 liquid-solid mass ratio, the paste was poured into a 3 cm × 3 cm × 5 cm test mold, the samples are cured at standard temperature curing, compressive strength tests were carried out when the test block had cured for 3, 7, and 28 days.

The mineral composition of the sample was analyzed using a D/Max 2200 XRD (Rigaku, Tokyo, Japan). The degree of hydration was analyzed with a TG/DSC1/1600 (Mettler, Inc., Toledo, OH, USA). The degree of polymerization of silicon oxides was determined with a FTIR (Perkin Elmer, USA). The morphologies and properties were observed with a SEM (JEOL, Tokyo, Japan). The pore structure was determined with an MIP (Georgia, USA).

Results and discussion

Analysis of sample compressive strength

The mixing proportions of cement and CGR pastes are shown in tab. 3. From fig. 3, it can be seen that the compressive strength of C1 was low. The compressive strengths of C2-C5 were enhanced to a certain extent compared with C1, and the compressive strengths of C2 were 6.3 MPa, 10.8 MPa, and 12.3 MPa. The HSW has significantly effect on the property of pastes, the highest increase in compressive strength was found at 3 days. As some literature have reported that increasing activator concentration leads to an increase in mechanical strength of alkali-activated cementitious materials [9].

Table 3. Ratios of ecological cementitious materials paste

Mixture number	CGR [%]	Cement [%]	Tap water [%]	HSW [%]	Curing method
C1	90	10	100	0	Standard curing
C2			75	25	
C3			50	50	
C4			25	75	
C5			0	100	

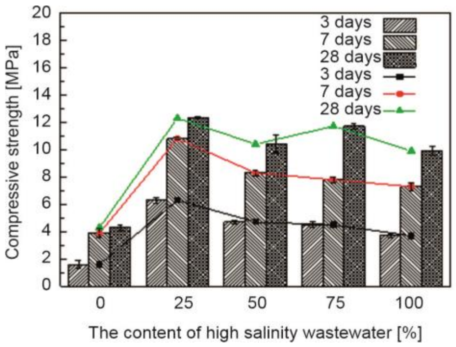

Figure 3. Compressive strength of cementitious materials under standard curing condition

The XRD analysis of samples

Figures 4 and 5 show XRD of pastes with different concentration of HSW. The hump of the CGR in Mix C1 significantly decreased, it indicates that the amorphous phases might have involved in the geopolymerization reaction. Small amounts of AFt (ettringite ($Ca_6Al_2(SO_4)_3(OH)_{12}$•$26H_2O$))and the calcium silicate hydrates (C-S-H(I)) gels were detected in the Mix C1. There were more C−S−H(I) and Friedel's salts were formed in the Mix C2, the intensity of these peaks increased slightly with ages. It indicated that the Mix C2 was an appropriate concentration of HSW. The generated of NaCl showed an increasing trend, and there was no diffraction peak of Na_2SO_4 in all systems, this indicated that NaCl in the samples was excessive and did not participate in the reaction completely. As reported in the literatures, the Na_2SO_4 and $CaCl_2$ can increase the pozzolanic reactivity of fly ash, and the NaCl did not result in substantial improvements to strength. The addition of excessive HSW may lead to the precipitation of NaCl, which would damage the integrity and strength of the sample.

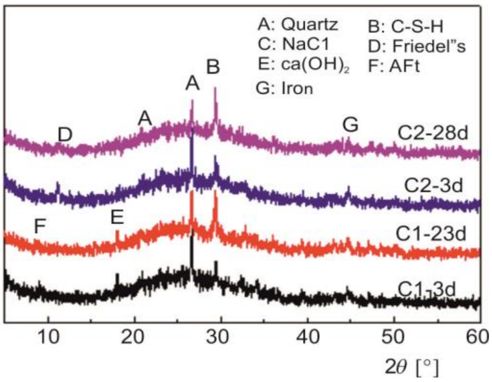

Figure 4. The XRD of C1 and C2 curing at 3 and 28 days

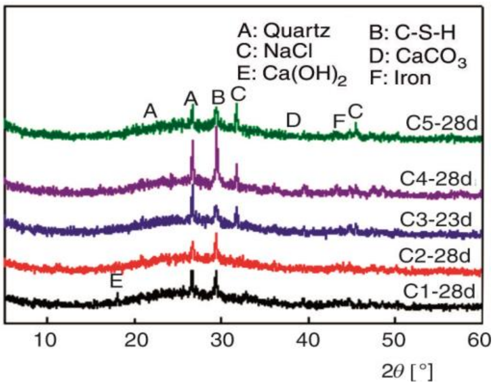

Figure 5. The XRD with HSW at 28 days

The FTIR analysis of samples

The FTIR spectra of the CGR and the CGR-based cementitious material cured for 28 days are shown in fig. 6, the FTIR spectrum frequencies and band assignments for gels C1 and C2 are shown in tab. 4. The main band corresponding to Si–O bond was observed in the region of 800-1300 c/m, As reported in the research literatures, it was mainly attributed to a C–S–H gels (Si–O) or the second component to the remains of a silica-rich gel. A more fuller study of the region was conducted on the spectra to obtain a clearer understanding of the introduction of HSW in the materials to identify the phases in the range of this band. The main band in the region was deconvoluted and the results of signal deconvolution for certain selected gels (C1 and C2) was shown in fig. 7, the frequency values and respective areas of the band found by deconvoluting for C1 and C2 was shown in tab. 5.

As shown in previous studies, the relative strength of the infrared absorption peak can be used to characterize the contents of the sample. The shift of the peak position can indicate that the polymerization degree of the group has changed and the shift from high wave number to low wave number indicates that the degree of polymerization for the group has decreased. The Band 1, Band 2, and Band 3 identified in fig. 7 are associated to the C–S–H, Q^3, and C–A–S–H (high calcium system). As compared with the system C1, the asymmetric

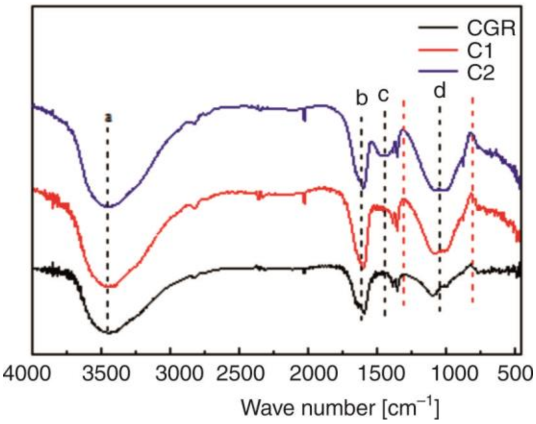

Figure 6. The FTIR spectra of C1 and C2 at 28 days

T–O vibration peak at 1030 cm^{-1} moved to 1039 cm^{-1} in the system C2, and the peak intensities increased. The HSW enhanced the area of band 1 from 16.0% to 25.0% when the tap water in system C1 was replaced by the HSW, indicating that the HSW could increase the activation of CGR and promoting the formation of C–S–H gels. The area of Band 2 was reduced from 56.5% to 44.9%, indicating that the HSW could promote the depolymerization of CGR and release active Si and Al to participate in hydration reaction with Ca^{2+}. The Si–O stretching vibration band of CGR appeared at around 1030 cm^{-1} may superpose upon the Si–O band of C–S–H, thus, the Si–O stretching vibration band shifts toward lower frequencies. The area of Band 3 increased from 27.5 to 30.1 indicating that the HSW could promote the formation of C–A–S–H gels to enhance the compressive strength of pastes, the content of C–S–H and C–A–S–H hydration products were higher than that in the system C1, this may be part of the reason that a higher compressive strength was observed from the C2 addition with HSW.

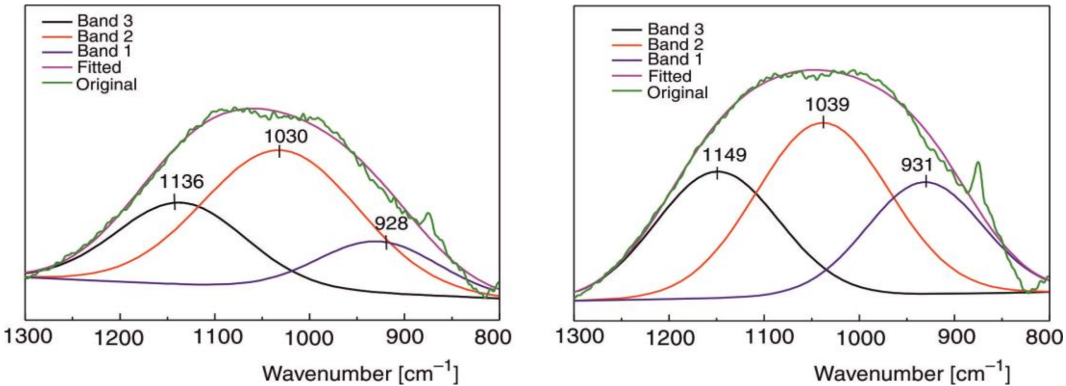

Figure 7. The DE convolution of selected FTIR spectra (800-1300 cm^{-1}) in fig. 6

Table 4. Frequency position [cm^{-1}] and area [%] of the deconvoluted components in C–S–H gels

Band	Gel C1 (cm^{-1})	Assigned to	Gel C2 (cm^{-1})	Assigned to
a	3449	O-H (H_2O)	3459	O-H (H_2O)
b	1588	H-O-H (H_2O)	1598	H-O-H (H_2O)
c			1454	C-O (CO_3^{2-})
d	1030	Si–O (C-S-H)	1039	Si–O (C-S-H)

The TG/DTG analysis of samples

The weight loss and derivative weight loss curves in the range 50-1000 °C for the C1 and C2 samples are shown in fig. 8. It can be seen that the C1 and C2 have a weight loss

Table 5. Frequency position [cm^{-1}] and area [%] of the deconvoluted components in C–S–H gels

Bands	C1		C2	
	V [cm^{-1}]	Area [%]	V [cm^{-1}]	Area [%]
Band 1	928	16.0	931	25.0
Band 2	1030	56.5	1039	44.9
Band 3	1136	27.5	1149	30.1

about 100-300 °C, which was mainly caused by the removal of free water or dehydration of hydrated calcium silicate gels (C–S–H) [10], but this peak could also be due to a small amount of dehydration from ettringite. The weight loss centered from 300-600 °C was due to the decomposition of $Ca(OH)_2$ which proved the further dehydration of C–S–H. The weight loss from 650 °C to 770 °C was caused by the decomposition of calcium carbonate ($CaCO_3$), and the weight loss from 770 °C to 950 °C was caused by the crystallization of C-S-H gels to from C–A–S–H gels. From the DTG analysis results of tab, 6, the C–S–H gels generated in the system C1 and C2 at 28 days increased from 3.23% to 4.61%, the enhancing rates is about 43%.

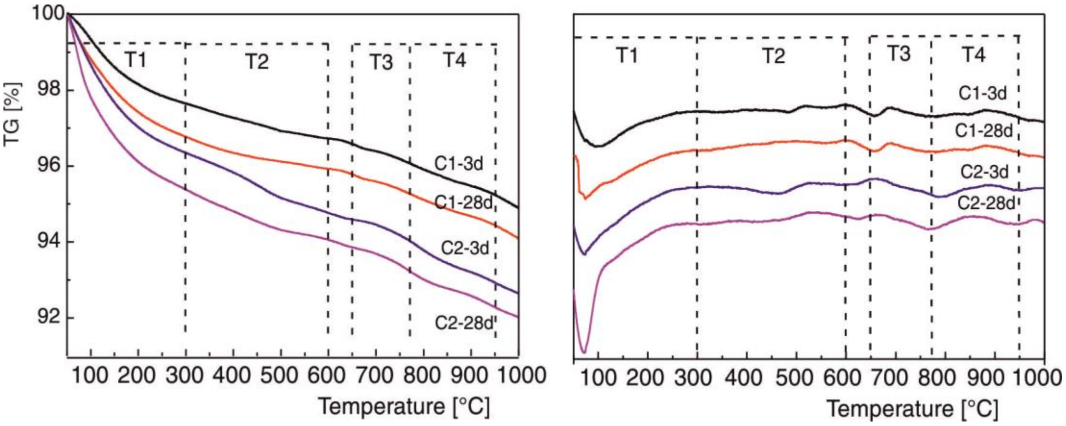

Figure 8. The TGA and DTG of C1 and C2 after 28 days

Table 6. Content of free water, C–S–H and $CaCO_3$ in ecological cementitious materials [wt.%]

Sample	T1	T2	T3	T4
	Free water and C–S–H	$Ca(OH)_2$	$CaCO_3$	C–A–S–H
C1-3 day	2.34	0.95	0.53	0.86
C1-28 day	3.23	0.87	0.53	0.87
C2-3 day	3.65	1.65	0.59	1.18
C2-28 day	4.61	1.40	0.66	1.03

The MIP analysis of samples

The effect of HSW on the interaction of CGR, Portland cement, and HSW in terms of C–S–H formation was also studied by the changes in the pore distribution and structure. The pore structure of tap water and 25% HSW mixed specimens with CGR and Portland cement were analyzed using MIP and the results are shown in fig. 9 and tab. 7. The pore size distribution of C2 revealed lower pore volume at any pore diagram range than that of C1, it can be related to the formation of low Ca/Si C–S–H(I) gels as well as formation of Friedel's salt. As reported in the previous literature, the densification of micro-structure may probably due to due to formation of C–S–H and Friedel's salts [11].

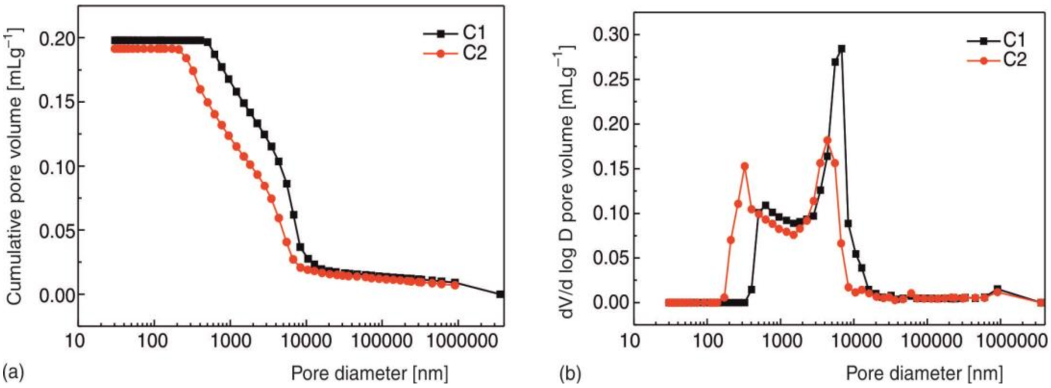

Figure 9. Curves of cumulative pore size distribution and differential pore size distribution

The pore in cementitious material can be roughly divided into four types according to the size of the pore: the gel pore (<10 nm), the transition pore (10-100 nm), capillary pore (100-1000 nm), and macropore (>1000 nm). As can be seen from tab. 7, as compared with C1, the proportion of macropores in C2 was decreased about 32.52%, and the number of capillary pores was increased about 96.88%. The addition of HSW can promote the transformation from macropore to capillary pores indicating that the structure of C2 became more denser than that of C1. It further proves that HSW can promote the hydration of cementitious materials.

Table 7. Pore size distribution of ecological cementitious materials

Mixture number	Porosity [%]	Most probable pore diameter [nm]	Pore diameter distribution [%]		
			10-100 [nm]	100-1000 [nm]	>1000 [nm]
C1	27.88	6806.99	0	20.21	79.79
C2	26.99	4343.22	0	39.79	60.21

The SEM analysis of samples

The micro-structures of C1 and C2 curing at 28 days are analysed by SEM and the image for samples were shown in fig. 10. The micro-structure of the C2 paste appeared to be more densified and networked than that corresponding to the C1 paste, and the following phenomenon being noticed:

- About C1, the surface of unreacted particles was dense, the hydration products were few, and the interface gap between unreacted particles and hydration products was large, greater number and size of pores.
- About C2, the surface of unreacted particles was corroded, the interface gap between unreacted particles and hydration products was large, and the zeolite phase was densely distributed on the surface of particles.

This indicating that the formation of gels was beneficial to the strength, the network structure of hydration products will be more compacter, and similar observations was reported by Shi *et al*. [12]. The C2 appeared to have a denser micro-structure and contained more gels and needles of what are probably C–S–H gels, ettringite and Friedel's salts, the connection between reaction products became more denser because of the hydration of Portland cement and formation of C–S–H gels.

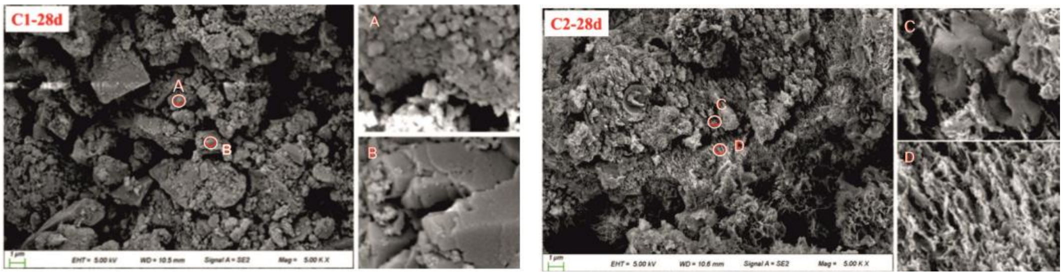

Figure 10. The SEM for C1 and C2 after 28 days with 5000 timesand 30000 times; (A)-(D)

Conclusions

- The CGR and HSW from CTC technology have the potential to be used as raw material and mixing water for cementitious material.
- When 25% HSW was used instead of tap water, the compressive strength of the paste was higher than that of without HSW, the enhancing rates was 294%, 177%, and 186% curing at 3, 7, and 28 days.
- With the appropriate amount of HSW introduced, the densification and strength of structure can be improved significantly, excessive HSW will cause a slight decreasing for density due to the precipitation of NaCl.
- With the addition of HSW, the pores distribution and structure were optimized, increasing the proportion of capillary pores and decreasing macropore to promote the microstructure more dense.

Acknowledgment

We acknowledge financial supports by Natural Science Foundation of Shaanxi Provincial Department of Education (20JY041) and Qing yuan Science and Technology Project (2020KJJH040).

References

[1] Shang, X., *et al*., Research Status and Prospects of Utilization Technologies of Slag From Coal Gasification, *Journal of Environmental Engineering Technology, 7* (2017), pp. 712-717
[2] Pomykala, R., The Mechanical Properties of Coal Gasification Residue as a Component of Concrete and Binding Mixtures, *Polish Journal of Environmental Studies, 23* (2014), 4, pp. 1403-1406
[3] Acosta, A., *et al*., Utilisation of IGCC Slag and Clay Steriles in Soft Mud Bricks (by Pressing) for Use in Building Bricks Manufacturing, *Waste Management, 22* (2002), 8, pp. 887-891
[4] Xie, J, *et al*., Technical Application of Safety and Cleaner Production Technology by Underground Coal Gasification in China, *J. Clean. Prod. 250* (2020), Mar., pp. 119-487
[5] Li, Z., *et al*., Structure Characteristics and Composition of Hydration Products of Coal Gasification Slag Mixed Cement and Lime, *Constr. Build. Mater. 213* (2019b), July, pp. 265-274
[6] Lee, C. Y., *et al*., Strength and Microstructural Characteristics of Chemically Activated Fly Ash-Cement Systems, *Cement and Concrete Research, 33* (2003), 3, pp. 425-431
[7] Mei, J., *et al*., Effect of Sodium Sulfate and Nano-SiO_2 on Hydration and Microstructure of Cementitious Materials Containing High Volume Fly Ash Under Steam Curing, *Construction and Building Materials, 163* (2018), Feb., pp. 812-825
[8] Shi, C., Day, R. L., Acceleration of the Reactivity of Fly Ash by Chemical Activation, *Cement and Concrete Research, 25* (1995), 1, pp. 15-21

[9] Gomaa, E., *et al*., Repair of Ordinary Portland Cement Concrete Using Ambient-Cured Alkali-Activated Concrete: Interfacial Behavior, *Cem.Concr. Res. 129* (2020), Mar., 105968

[10] Li, Y. L., *et al*., Thermal and Mechanical Properties of Alkali-Activated Slag Paste, Mortar and Concrete Utilizing Seawater and Sea Sand, *Constr. Build. Mater. 159* (2018), Jan., pp. 704-724

[11] Li, L. B., *et al*., Pore Structure Evolution and Strength Development of Hardened Cement Paste with Super Low Waterto- Cement Ratios, *Constr. Build. Mater. 227* (2019), Dec., 117108

[12] Shi, D., *et al*., Effects of Seawater on Mechanical Properties, Mineralogy and Microstructure of Calcium Silicate Slag-Based Alkaliactivated Materials, *Constr. Build. Mater., 212* (2019), July, pp. 569-577

Paper submitted: March 3, 2021
Paper revised: June 27, 2021
Paper accepted: July 9, 2021